Available online at www.sciencedirect.com

SciVerse ScienceDirect

Acta Materialia 61 (2013) 5105–5118

Acta MATERIALIA

www.elsevier.com/locate/actamat

Deposition behavior of thermally softened copper particles in cold spraying

Shuo Yin [a,b,*], Xiaofang Wang [a], Xinkun Suo [b], Hanlin Liao [b], Zhiwei Guo [b], Wenya Li [c], Christian Coddet [b]

[a] School of Energy and Power Engineering, Dalian University of Technology, Dalian 116024, Liaoning, People's Republic of China

[b] LERMPS (Laboratoire d'Etudes et de Recherches sur les Matériaux, les Procédés et les Surfaces), Université de Technologie de Belfort-Montbéliard, Site de Sévenans, 90010 Belfort Cedex, France

[c] Shaanxi Key Laboratory of Friction Welding Technologies, School of Materials Science and Engineering, Northwestern Polytechnical University, Xi'an 710072, Shaanxi, People's Republic of China

Received 18 December 2012; received in revised form 15 April 2013; accepted 16 April 2013
Available online 20 June 2013

Abstract

Finite-element analysis (FEA) combined with experimental observation was conducted on preheated Cu particles deposited on Cu substrate to clarify the deposition behavior of thermally softened particles in cold spraying. An explicit FEA code, ABAQUS, was used to predict the deformation features of the thermally softened particles. The experiment was performed by a home-made cold-spray system with a powder preheating device. Considering the possible serious oxidation of the cold-sprayed particles under high-temperature conditions, the preheating temperature was limited to 300 °C for each test. Based on the numerical and experimental results, a new concept called the thermal softening zone within which thermal softening occurs is proposed in the present work. It is found that thermally softened particles deform more intensively compared to non-preheated particles, and a more prominent metal jet can be achieved at the rim of the deformed particles with higher initial temperature. Moreover, the results also reveal that increasing the particle preheating temperature can stimulate the occurrence of thermal softening. For non-preheating or low-temperature preheating particles, thermal softening mainly occurs at the interfacial region. If the preheating temperature is sufficiently high, the whole particle can experience thermal softening. In addition, it is also found that preheated particles are more likely to deposit on the substrate surface than non-preheated particles. In addition, particle preheating is also found to facilitate the coating formation process, enabling the coating to be very thick. The coating microhardness decreases with increasing particle preheating temperature due to the elimination of work hardening by thermal softening.

Keywords: Cold spraying (CS); Deposition behavior; Particle preheating; Thermal softening; Numerical simulation

1. Introduction

Cold spraying (CS), also called cold gas dynamic spraying or kinetic spraying, is a relatively new material deposition technique, which has been developed for more than two decades. In this process, powder particles are accelerated to a high velocity normally ranging from 300 to 1200 m s^{-1} in a supersonic jet flow and projected onto the substrate or already deposited coating in an entirely solid state. Intensive plastic deformation induced by the high-velocity impact occurs in cold-sprayed particle, substrate (or already deposited coating) or both, enabling a low-oxidized cold-sprayed coating to be formed [1,2].

In general, particle velocity prior to the impact is an important factor for CS because the successful deposition of cold-sprayed particles relies only on the kinetic energy

* Corresponding author at: School of Energy and Power Engineering, Dalian University of Technology, Dalian 116024, Liaoning, People's Republic of China. Tel.: +33 605973500.
E-mail address: s.yin1984@hotmail.com (S. Yin).

1359-6454/$36.00
http://dx.doi.org/10.1016/j.actamat.2013.04.041

rather than the combined effect of both kinetic and thermal energies available in conventional thermal spraying. It has been widely accepted that there exists a unique critical velocity for a given condition (e.g. specific particle size, temperature and material properties), above which successful bonding can be achieved [3–5].

As for the bonding mechanism, a number of works have been carried out during the past decade to improve our understanding on this issue [3–15]. Currently, the most widely accepted view of the bonding mechanism can be regarded as the occurrence of adiabatic shear instability (ASI) at the interface which results from the high strain rate and the intensive localized deformation during the particle deposition process. At the region where ASI occurs, adiabatic heating-induced thermal softening is dominant over work hardening, and then metals behave like a viscous material, extruded from the interface, forming an outward metal jet at the rim [3,4]. This viscous-like metal jet helps to clean up the cracked native oxide film which originally exists on particle and substrate surfaces, allowing metal-to-metal contact and thus metallic bonding to occur [6].

Mechanical interlocking and metallurgical bonding are commonly perceived to be two dominant mechanisms of metallic bonding in CS. It was proposed by Grujicic et al. that the interfacial instability occurring during the high-velocity impacting process results in material roll-ups and vortices at the interface, as a consequence, substrate and coating materials mix at the interface region, leading to mechanical interlocking [7]. Experimental observations of Cu–Al [16] and Zn–Al [17] mixtures at the interface, in previous literature, provide strong evidence for the mechanical interlocking mechanism in CS. In addition, Hussain et al. proposed another conception of mechanical interlocking, namely that the formation of substrate jet partially envelops the particle and enables the deposited particle to be locked by the substrate material [13]. Metallurgical bonding is normally known as a result of the atomic diffusion between different materials, which can provide better bonding strength compared to mechanically based bonding. The formation of intermetallic phase at the interfacial region is recognized as a marker for oxide-free interface, the occurrence of diffusion and true metallurgical bonding [18–20]. In some experimental studies, relatively thick intermetallic layers (several hundreds of nanometers) have been indentified at different interfaces, e.g. $NiAl_3$ [21,22], $MgZn_2$, $Mg_5Zn_2Al_2$, $Mg_{11}Zn_{11}Al_6$ [17], Al_2Cu_3, Al_2Cu [10], $AlCu_4$, Al_4Cu_9, AlCu, Al_2Cu, Al–Al_2Cu [23], Al_2Cu, Al_4Cu_9 [14], Al_2Cu [24] and Al_5Fe_2 [25,26]. Additionally, previous literatures have also reported that the formation of intermetallic phase is always accompanied with transient interfacial melting, because the solid-state diffusion speed is too low to form a sufficiently thick intermetallic layer as observed in the experiments under the extremely short timescale of the particle–substrate reaction in CS [14,23,24].

The temperature of cold-sprayed particles prior to the impact is always far lower compared to the material melting point because the particles can only be heated up over an extremely short duration by the driving gas during the CS process. Accordingly, the cold-sprayed coating is characterized by low oxidation, retaining the original mechanical properties to a great extent. However, for the same reason, the bonding strength between certain cold-sprayed particles, e.g. hard particles or larger particles, and substrate (or already deposited coatings) cannot be guaranteed. In some works, it is reported that heating the powder particles to a suitable temperature range before spraying can decrease the critical velocity and increase the bonding strength as well as the deposition efficiency, especially for those materials which are difficult to successfully deposit by the conventional CS process [27,28]. Kim et al. found that, in warm spraying in which powder particles can be heated to a temperature normally around $0.5T_m$, extremely fine grains (several tens of nanometers) can be formed along the particle–substrate interfacial boundary and even within the whole splat and possibly the final fully nanocrystalline metallic coating duo to the dynamic recrystallization, which significantly enhances coating quality [29–31]. Although there already exist some meaningful findings, currently the deformation behavior of the preheated cold-sprayed particles is still not well known. In this study, therefore, numerical simulation combined with experimental observation is performed to clarify the deposition characteristics between thermally softened particle and substrate. Furthermore, the deformation character of the particles inside the cold-sprayed coating is also discussed to study the effect of particle preheating on the coating formation process.

2. Experimental details

Cold-sprayed splats and coatings were produced by using a home-made CS system (LERMPS, UTBM, France) with an optimal de-Laval type converging–diverging nozzle. The nozzle has a rectangular cross-section with an expansion ratio of about 3.8. For all tests, high-pressure compressed air was used as the carrier gas with the inlet pressure and temperature of 2.5 MPa and 500 °C, respectively. The standoff distance from the nozzle exit to the substrate surface was 30 mm. A high gun traverse speed of 500 mm s^{-1} was used to produce the individual cold-sprayed splat, and a low gun traverse speed of 100 mm s^{-1} was employed for the full coating deposition. Because air was chosen as the carrier gas, the oxidation of the powder particles during the preheating process cannot be avoided. Serious oxidation can degrade the coating performance and thus weaken the advantages offered by "low-temperature" CS. On the other hand, thick oxide film on the particle surface significantly hinders the bonding between the particles and the already formed coating or substrate [31,32]. Therefore, in order to reduce the negative influence by the oxidation, the particle preheating temperature in this study was limited to only 300 °C. Based on this fact, four preheating temperatures were tested: 25, 100, 200 and 300 °C.

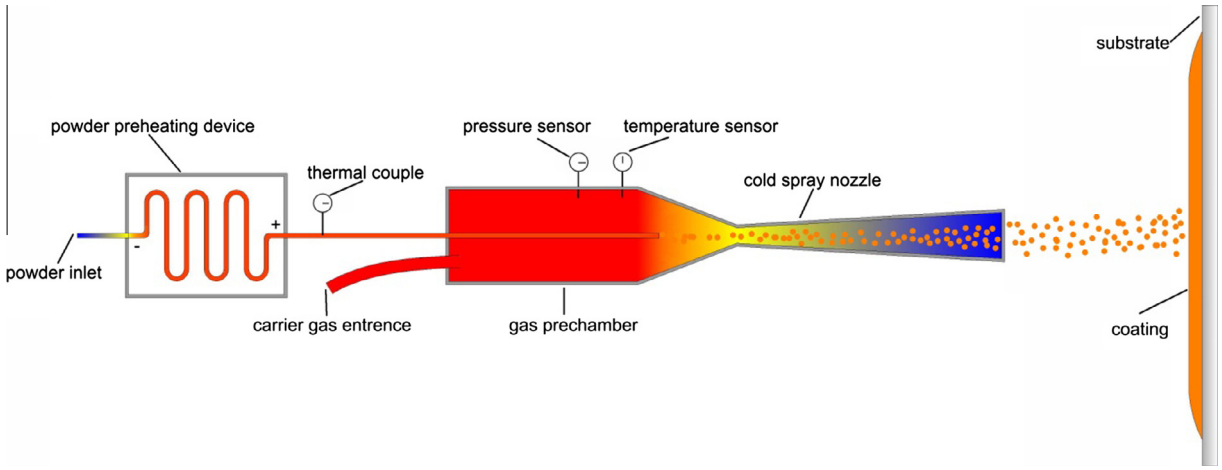

Fig. 1. Schematic of the CS system with the powder preheating device.

Powder particles were preheated by a home-made preheating device before being injected into the nozzle. The schematic of the CS system with the preheating device used in the experiment is illustrated in Fig. 1. As can be seen, powders were firstly injected into the preheating device inside which a long coiled tube is installed in order to to achieve particle heating. The electrodes were placed at both sides of the coiled tube to heat the tube wall and thus the gas flowing through the tube. The gas temperature was controlled by adjusting the voltage and measured by the thermal couple located near the tube outlet. When the desired gas temperature was reached, powders were released and heated up during the travel period through the tube. Because the tube was manufactured with sufficient length, particles have adequate heating time and hence achieve the roughly same temperature as the gas after leaving the preheating device.

Pure Cu powder with a spherical morphology was selected as the feedstock. The powder size distribution was measured to be between 0 and 150 μm with 75 μm average particle diameter by a laser diffraction sizer (Mastersizer 2000, Malvern Instruments Ltd., UK). Fig. 2 shows both the powder size distribution and the scanning electron microscopy (SEM) morphology of the Cu powder used in this experiment. Polished and grit-blasted Cu plates were employed as the substrate for individual splat deposition and full coating deposition, respectively.

The powder and coating microstructures were examined by optical microscopy (OM) (Nikon, Japan) and SEM (JSM5800LV, JEOL, Japan). The coating microhardness was tested by a Vickers hardness indenter (Leitz, Germany) with a load of 200 g for 30 s. More than 15 values were randomly tested and averaged to evaluate the hardness. The surface temperature of the coating was measured and simultaneously recorded by an imaging infrared camera (Agema Thermovision 470). Thermal infrared images were continuously recorded with a video system and then analyzed by camera software, enabling the detailed investigation on the temporal temperature development of the coating surface temperature during the CS process.

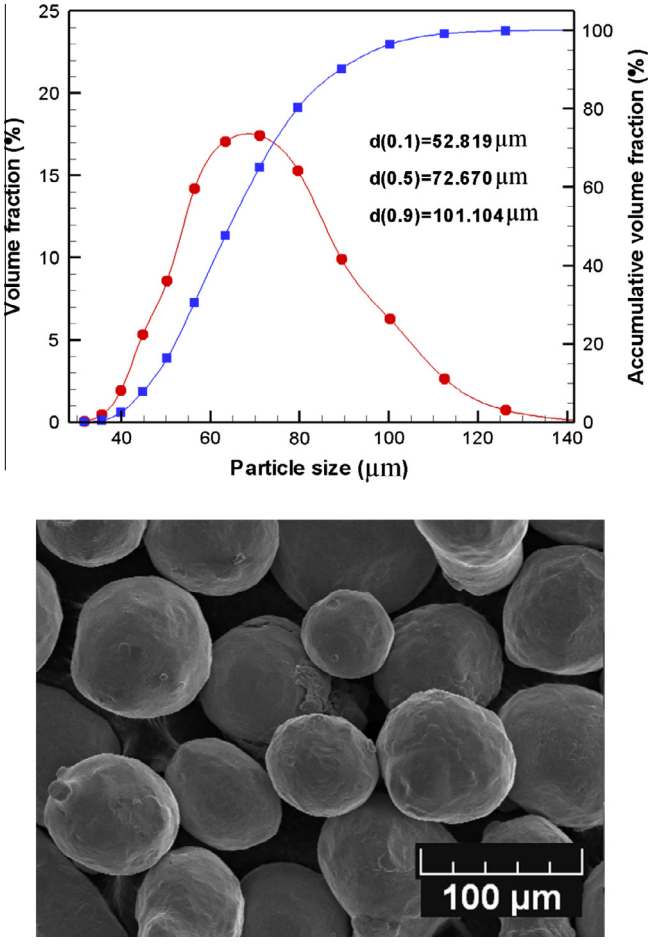

Fig. 2. Powder size distribution and SEM morphology of the Cu powders.

3. Computational descriptions

3.1. Numerical model

The high-velocity impacting process is modeled by using an explicit finite-element analysis (FEA) code, ABAQUS

[33], with the Lagrangian algorithm which has been widely used in previous studies [3,4,11,12,24,31]. Both single-particle and multi-particle impacts are considered in this study. All the impacting processes are assumed to be an adiabatic process and the dynamic explicit procedure (Dynamic-Explicit) is performed to realize the adiabatic stress analysis. Due to the axially symmetric character of the single-particle impact, such models are simplified as axisymmetric models in order to reduce the computational time. All the particles have a diameter (d_p) of 20 μm. The radius and height of the substrate are defined as four times larger than the particle diameter. The geometries are partitioned by the four-node bilinear axisymmetric quadrilateral elements with reduced integration and hourglass control (CAX4R). The axisymmetric condition is applied to the symmetric axis and the fixed boundary condition is enforced to the bottom and lateral. For multi-particle impact, three sizes of randomly distributed particles are considered, namely 10, 20 and 30 μm. The radius and height of the substrate are defined as 400 and 200 μm, respectively. Four-node linear plane strain quadrilateral elements (CPE4) are adopted to characterize the deformation in the central cross-section. The fixed boundary condition is enforced to the bottom and lateral. All the contact processes are implemented by using the surface-to-surface penalty contact algorithm with balanced contact pair formulation. The computation domain, meshing and boundary conditions for single-particle impact are given in Fig. 3. For multi-particle impact, the meshing is partitioned in a similar way.

The initial particle velocities for different cases are chosen based on the principle of exceeding the correspondingly critical velocities. Therefore, the initial velocities for Cu particle on Cu substrate, Fe particle on Fe substrate, and Ni particle on Ni substrate are 600, 700 and 800 m s^{-1}, respectively, according to the calculated results by Bea et al. [11]. As for the particle temperature prior to the impact, our previous Computational Fluid Dynamics (CFD) results indicated that the particles can be slightly heated to 100–200 °C by the driving gas before they impact on the substrate [34]. Therefore, in this study, the particle initial temperature is set as 100 °C for the non-preheated particle. For preheated particle, the initial temperature varies from 200 to 800 °C. Additionally, the substrate temperature is taken as 25 °C for all cases.

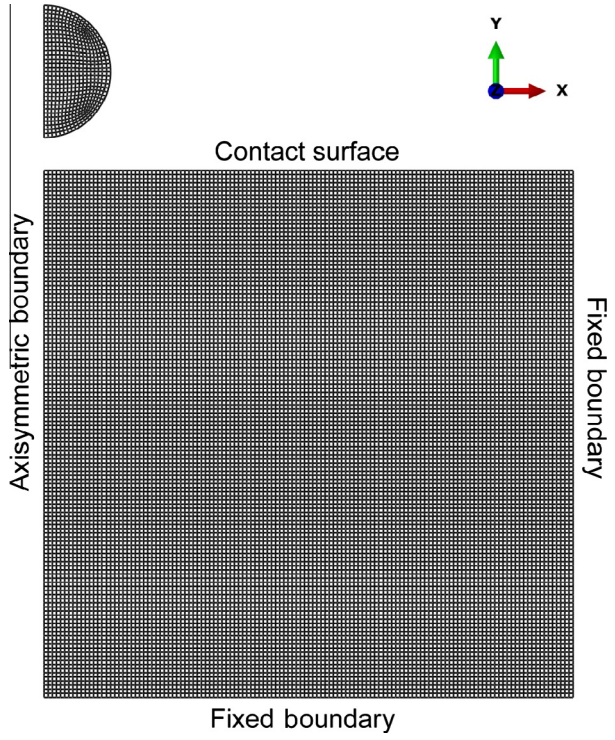

Fig. 3. Computation domain, meshing and boundary conditions for the single-particle impacting process.

3.2. Material model

The particles and substrate are described as a Johnson and Cook plasticity model which accounts for strain, strain-rate hardening, as well as thermal softening. The stress is expressed according to the von Mises plasticity model. The yield stress (σ_y) of the material is expressed as follows [35]:

$$\sigma_y = [A + B(\varepsilon_e^p)^N][1 + C\ln\dot{\varepsilon}^*][1 - (T^*)^M], \quad (1)$$

where A, B, N, C and M are material-related constants, ε_e^p is the effective plastic strain, and $\dot{\varepsilon}^*$ is the effective plastic strain rate normalized with respect to a reference strain rate. T^* is a non-dimensional temperature defined as:

$$T^* = \frac{T - T_0}{T_m - T_0}, \quad (2)$$

where T_m is the melting temperature and T_0 is a reference temperature. A linear Mie–Grüneisen equation of state (EOS) is employed for the elastic behavior. The mechanical and thermal properties are assumed to be isotropic. The properties of the metals used in this study are listed in Table 1.

Table 1
Material properties of the metals used in this simulation.

	Fe	Ni	Cu
Density, ρ (kg m^{-3})	7890	8900	8960
Shear modulus, G (GPa)	80	79	46.3
Elastic modulus, E (GPa)	207	207	124
Poisson's ratio, v	0.29	0.31	0.34
Specific heat, C_p (J kg^{-1} $°C^{-1}$)	452	456	383
Yield strength, A (MPa)	175	167	90
Hardening coefficient, B (MPa)	308	648	292
Strain-hardening exponent, N	0.32	0.33	0.31
Strain rate constant, C	0.06	0.006	0.025
Softening exponent, M	0.55	1.44	1.09
Melting temperature, T_m (°C)	1538	1478	1083
Reference temperature, T_0 (°C)	25	25	25
Reference strain rate (s^{-1})	1	1	1
Sound velocity, C_0 (m s^{-1})	3574	5060	3490
Slope in v_s vs. v_p, S	1.92	1.5	1.49
Grüneisen coefficient, γ_0	1.69	2.0	2.02

4. Results and discussion

4.1. Particle deformation behavior

Fig. 4 shows the contours of the temperature and effective plastic strain of a single Cu particle depositing on a Cu substrate with different particle initial temperatures. Obviously, with the increment in particle initial temperature, the particle experiences increasingly intensive deformation and the metal jet formed at the rim of the flattened particle becomes more and more prominent. It is believed that the enhanced thermal softening effect caused by the increasing initial temperature is the main reason for this phenomenon. The detailed interpretation for this fact will be discussed in the following section. It is also noticed that the localized plastic deformation occurs at the periphery of the contact interface, where the temperature is much higher than the inner part of the particle due to plastic dissipation-induced adiabatic temperature rise. The same deformation character and variation tendency also can be found in the cases of Fe particle on Fe substrate as shown in Fig. 5 and Ni particle on Ni substrate as shown in Fig. 6. Fig. 7 shows the compressional ratio of the cold-sprayed particle vs. the particle initial temperature for various metals, where compressional ratio is defined as $(d_p - h_f)/d_p$ and is used to describe the extent of deformation, where h_f is the deformed particle height. It is clear that the compressional ratio demonstrates an obviously upward trend with the particle temperature regardless of the metal types, which further indicates that the increase in the particle initial temperature does in fact contribute to the deformation of cold-sprayed particles.

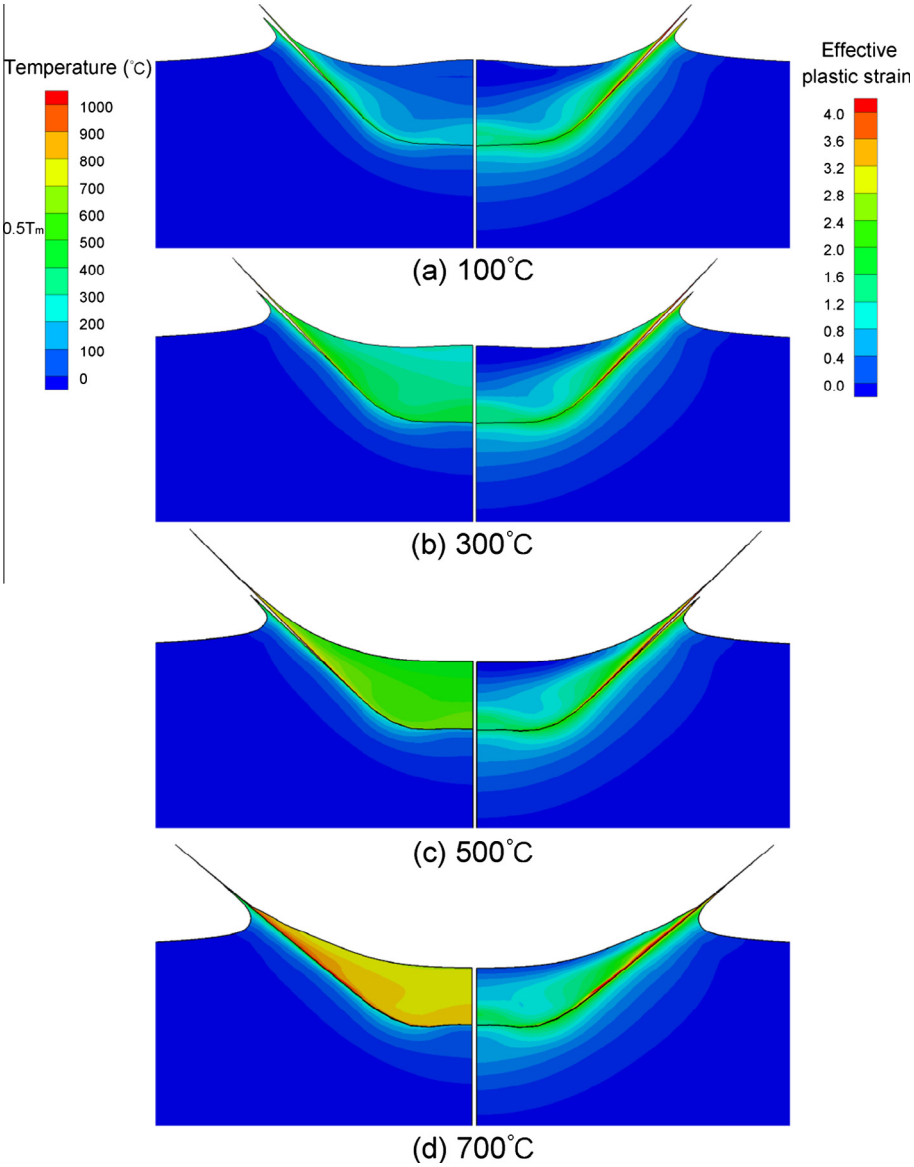

Fig. 4. Contours of the temperature and effective plastic strain of a single Cu particle depositing on a Cu substrate with different particle initial temperatures: (a) 100 °C, (b) 300 °C, (c) 500 °C and (d) 700 °C.

Fig. 8 shows the simulation results of the temperature distribution of several Cu particles depositing on a Cu substrate with different particle initial temperatures. As can be seen in Fig. 8a, the top layer particles mainly deform at the lower part and the temperature rise at the corresponding region is relatively high as a result of the adiabatic heating. However, it is worth noting that the temperatures of the former deposited particles are higher compared to the top layer particles, especially at the particle upper part, due to the subsequent impact of further deposited particles. In addition, the temperature distribution within the former deposited particles is more uniform in comparison with the top layer particles. This fact indicates that the inner part of the coatings may achieve better bonding strength compared to the outer part. Similar deformation features also can be found in Fig. 8b and c. Furthermore, it is also noticeable from Fig. 8 that the deposited particles flatten more and more remarkably as the initial temperature increases gradually.

4.2. Thermal softening effect

It is know that when metals deform at a sufficiently high temperature, necessarily greater than $0.4–0.5T_m$ [36], a series of changes, such as dynamic recovery and dynamic recrystallization, will take place within the metals, significantly influencing the deformation process [37]. Such changes can eliminate the work-hardening effect which results from the dislocation density increment and dislocation proliferation occurring during the plastic deformation process by the means of dislocation climbing, dislocation cross-slips and new grain growth, enabling the metal materials to soften. This phenomenon is normally termed the thermal softening effect. If the thermal softening effect dominates the work-hardening effect, the metal flow stress starts to become stable and plastic flow occurs, resulting in the metals behaving like a viscous material. Based on the above discussion, it is not difficult to consider that only when the temperature exceeds the critical temperature

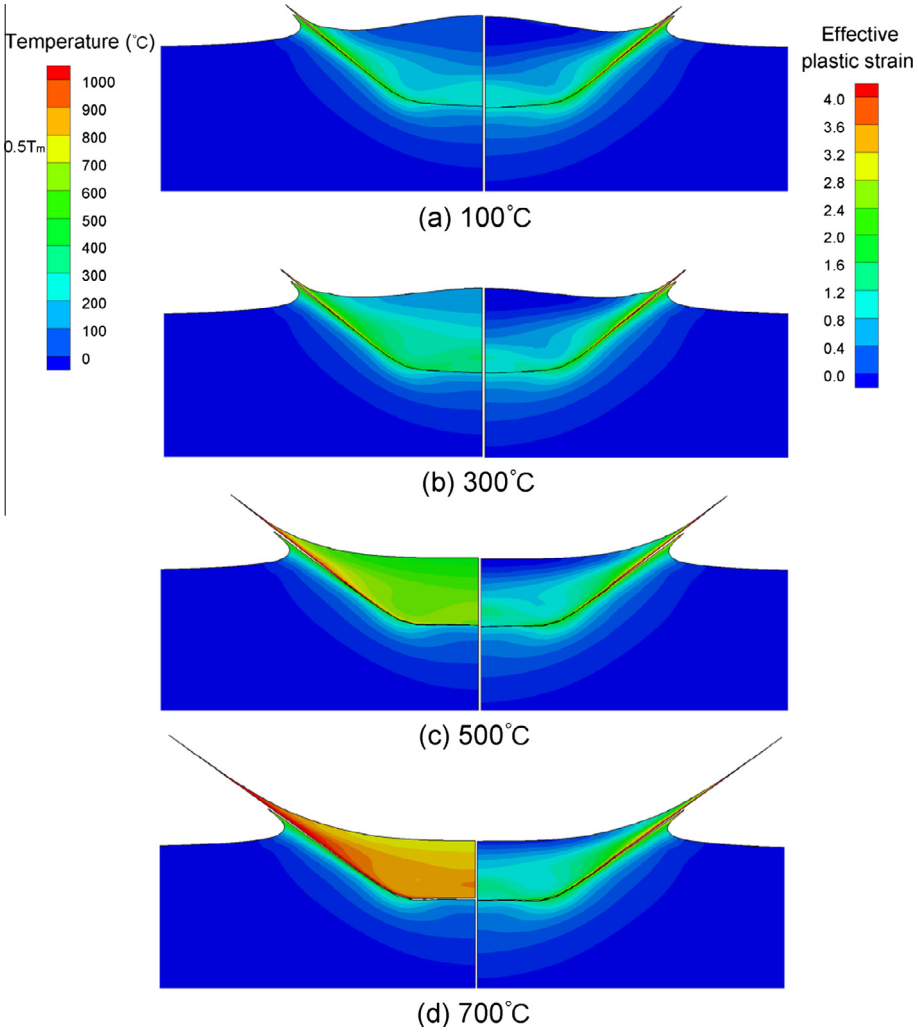

Fig. 5. Contours of the temperature and effective plastic strain of a single Fe particle depositing on a Fe substrate with different particle initial temperatures: (a) 100 °C, (b) 300 °C, (c) 500 °C and (d) 700 °C.

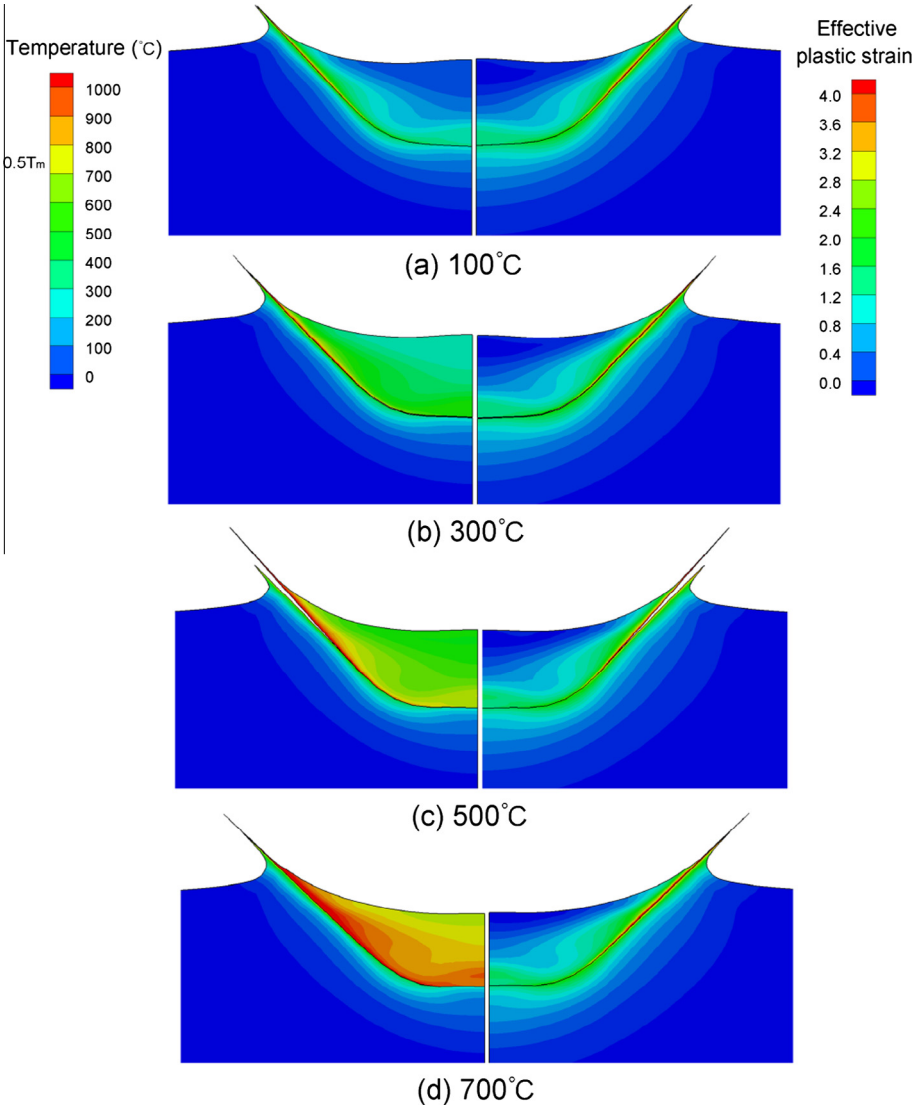

Fig. 6. Contours of the temperature and effective plastic strain of a single Ni particle depositing on a Ni substrate with different particle initial temperatures: (a) 100 °C, (b) 300 °C, (c) 500 °C and (d) 700 °C.

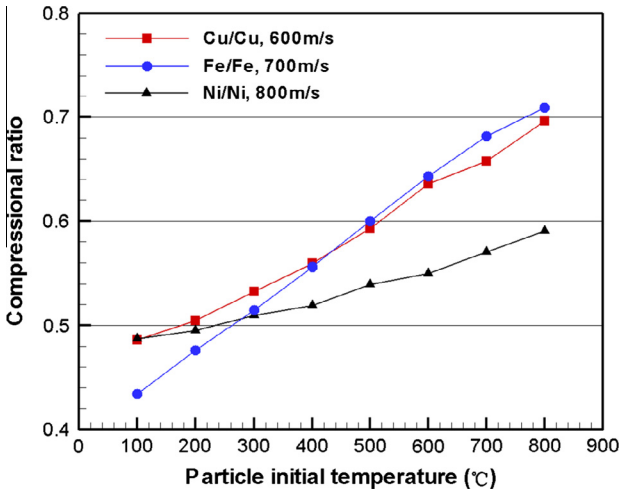

Fig. 7. Particle compressional ratio vs. the particle initial temperature.

range (0.4–$0.5T_m$), can dynamic changing, in other words, thermal softening, be triggered. In this case, $0.5T_m$ can be reasonably regarded as a criterion for the occurrence of thermal softening. In conventional CS without particle preheating, when the adiabatic heating-induced thermal softening effect is dominant over the work-hardening effect, ASI can occur and the metal jet then forms [3]; as a result, the metal-to-metal contact as well as the metallic bonding can be expected between particles and substrate. However, if particles are preheated before spraying, not only the adiabatic temperature rise, but also the particle initial temperature contributes to the particle final deposition temperature. Therefore, it can be considered that the combination of the particle initial temperature and the adiabatic temperature rise determines whether the local temperature can reach the critical criterion ($0.5T_m$) and thermal softening can occur.

In order to evaluate the possibility of the occurrence of thermal softening during the CS process when particles are

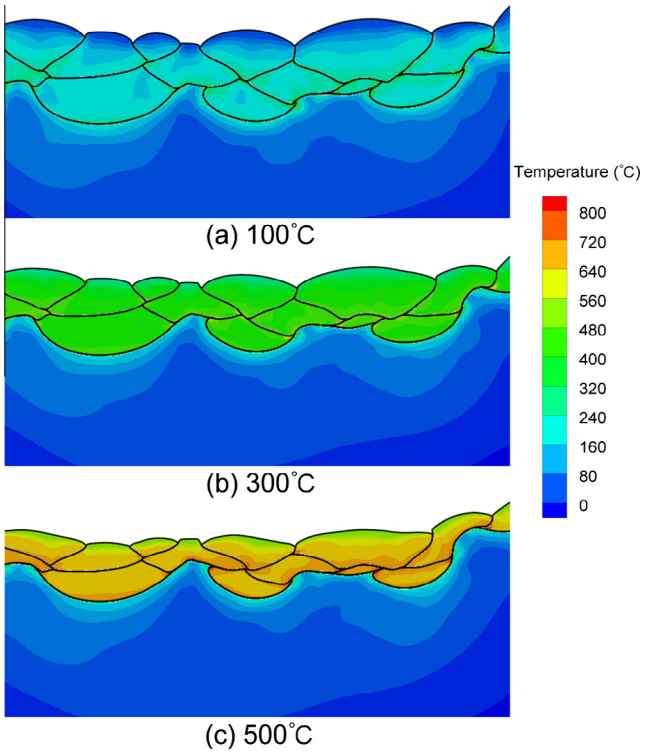

Fig. 8. Contours of the temperature of several Cu particles depositing on a Cu substrate with different particle initial temperatures: (a) 100 °C, (b) 300 °C and (c) 500 °C.

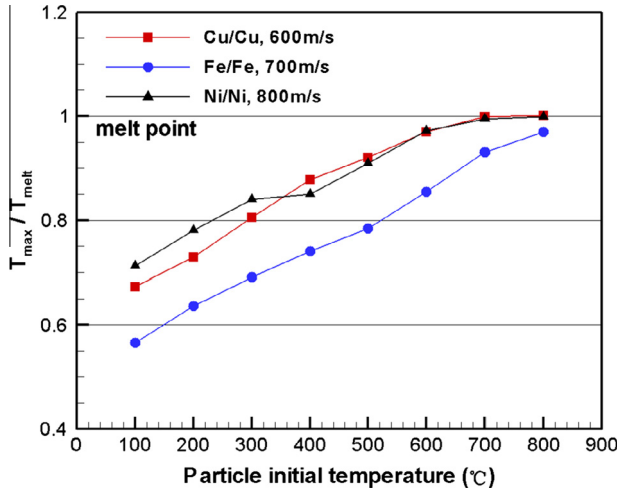

Fig. 9. Particle local maximum temperature vs. the particle initial temperature.

preheated before spraying, the particle maximum temperature and temperature rise vs. the particle initial temperature are provided in Figs. 9 and 10. As can be seen, the particle maximum temperature shows an upward trend with increasing particle initial temperature, but the maximum temperature rise decreases gradually. It is known that the local maximum temperature is caused by the combination of both particle initial temperature and maximum adiabatic temperature rise. Here the maximum temperature rise

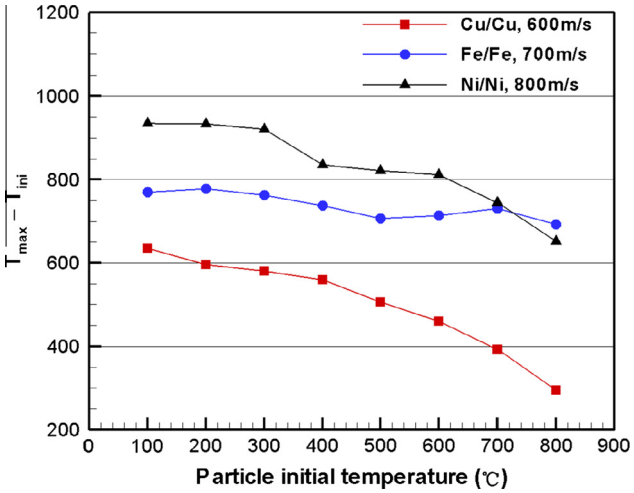

Fig. 10. Particle maximum temperature rise ($T_{max} - T_{ini}$) vs. particle initial temperature.

decreases with increasing particle initial temperature, which means that the temperature rise contributes less and less to the particle final deposition temperature. Knowing this, one can easily conclude that it is the growing initial temperature that causes the increase in the local maximum temperature rather than the adiabatic temperature rise. The reason why the maximum temperature rise decreases will be discussed in detail in the following section. In addition, from Fig. 9, it is interesting to find that even for the non-preheated particle, the maximum temperature can exceed the critical temperature ($0.5T_m$) owing to the plastic dissipation-induced adiabatic temperature rise. This fact means that, in most cases, dynamic changing and thermal softening can occur during the CS process. Additionally, it is also found that the maximum temperature cannot reach the melting point for all temperatures.

In order to investigate further the thermal softening phenomenon within a preheated cold-sprayed particle, Figs. 4–6 are analyzed in detail. A new concept, the so-called thermal softening zone (TSZ) is proposed, which is defined as the local zone where the temperature is greater than $0.5T_m$. Inside the TSZ, thermal softening occurs and competes with work hardening, as a consequence, intensive deformation can be expected within the TSZ. As can be seen from Figs. 4–6a in which particles are non-preheated, the TSZ is very narrow and is localized along the contact interface boundary, which is mainly produced by the plastic dissipation-induced adiabatic temperature rise. As the particle initial temperature is gradually increased to 300 °C, the TSZ is not only limited to the interfacial narrow region, but spreads to the lower part of the particle. The experimental study of Kim et al. provided a TEM image showing that a refined grain resulting from the dynamic recrystallization is formed at the lower part of the particle during a warm-spraying process, which implies the occurrence of thermal softening, supporting the numerical results of the current paper [29,30]. Furthermore, when the particle temperature

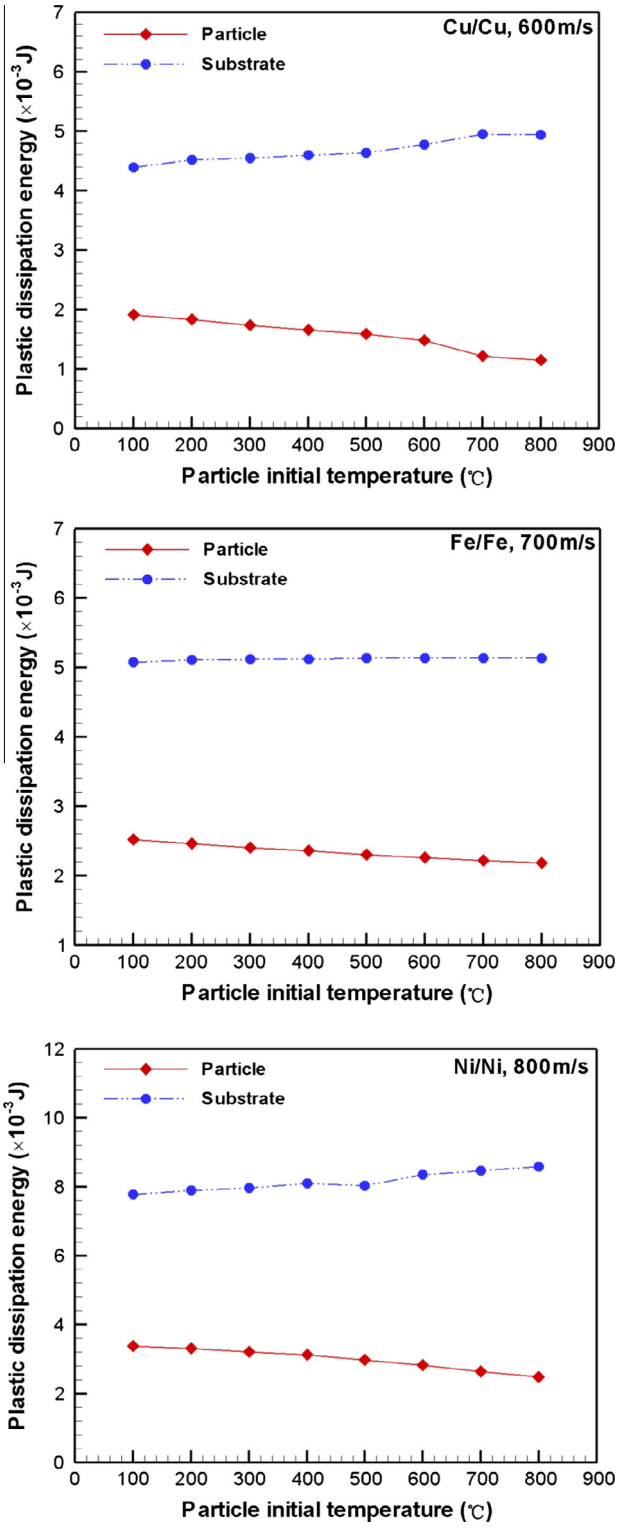

Fig. 11. Plastic dissipation energy of both cold-sprayed particle and substrate vs. the particle initial temperature: (a) Cu particle on Cu substrate at 600 m s^{-1}, (b) Fe particle on Fe substrate at 700 m s^{-1} and (c) Ni particle on Ni substrate at 800 m s^{-1}.

is increased to more than 500 °C, it can be seen that the whole particle almost reaches the critical temperature ($0.5T_m$), which suggests that the thermal softening effect works over the whole deformed particle. A similar phenomenon can also be found in Kim et al.'s study in which the whole splat experiences the grain refining process [30]. In addition, it is worth noting that the whole particle experiencing the thermal softening is mainly due to the particle preheating process rather than the adiabatic temperature rise, because the adiabatic heating plays a key role only at the extremely deformed zone (interfacial zone). Moreover, as for the full coating shown in Fig. 8, it is found that the area of the TSZ of the particles inside the coating is larger than that at the top layer due to the subsequent impacting, which implies that the inner particles are more likely to experience thermal softening.

4.3. Energy distribution

During the particle deposition process, the initial kinetic energy (E_U) can convert into four sorts of energies, namely plastic dissipation energy (E_P), viscous dissipation energy (E_V), frictional heat (E_F) and recoverable elastic strain energy (E_R), which can be expressed as follows [33]:

$$E_U = E_P + E_V + E_F + E_R$$

In the work of Bea et al. [11], the plastic dissipation energy, viscous dissipation energy and frictional heat are considered to contribute to the adhesion energy, while the elastic strain energy is regarded as the rebound energy. Moreover, the viscous dissipation energy and frictional heat are relatively small compared to the plastic dissipation energy, hence Bea et al. use plastic dissipation energy and elastic strain energy as a comparison to evaluate the bonding and rebounding between particles and substrate. In this study, plastic dissipation energy is also chosen to quantitatively evaluate the plastic deformation of both particle and substrate. Fig. 11 demonstrates the plastic dissipation energies of both particle and substrate vs. the particle initial temperature. Interestingly, unlike the changing trend of deformation extent as discussed in Section 3.1, the particle plastic dissipation energy decreases gradually with increasing particle initial temperature, while the energy dissipated into the substrate shows a reverse trend. The reason for this difference can be interpreted as follows. As we know, plastic dissipation energy is due to the dissipation of plastic work during the deformation process. When metals get into a thermal softening state, work hardening will be gradually eliminated by thermal softening. The more intensive the thermal softening is, the more completely the work hardening can be eliminated and the less plastic work is needed for deformation. If the thermal softening effect completely dominates the work-hardening effect, the plastic flow stress becomes stable and no longer increases, but the plastic strain nevertheless proceeds. Particles with high initial temperature can easily undergo thermal softening [30] and hence can maintain the thermal softening and even the plastic flow state for a long time. Accordingly, only less plastic work can lead to the relatively larger plastic deformation.

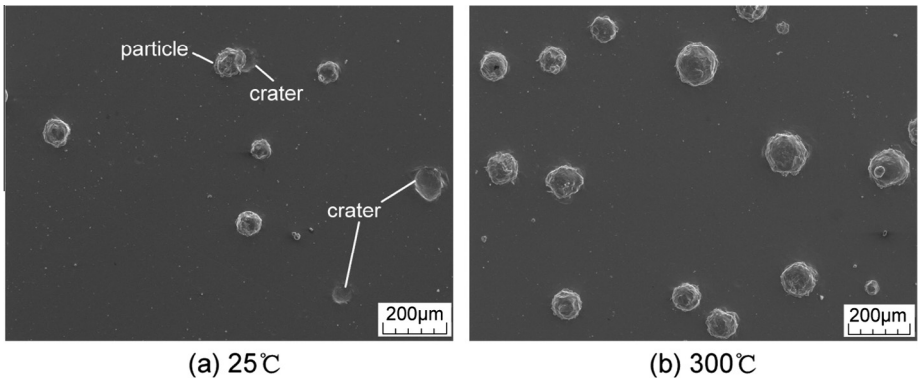

Fig. 12. Surface morphologies of the substrate following impact of several individual Cu particles with and without preheating treatment: (a) non-preheating with a temperature of 25 °C and (b) preheating with a temperature of 300 °C.

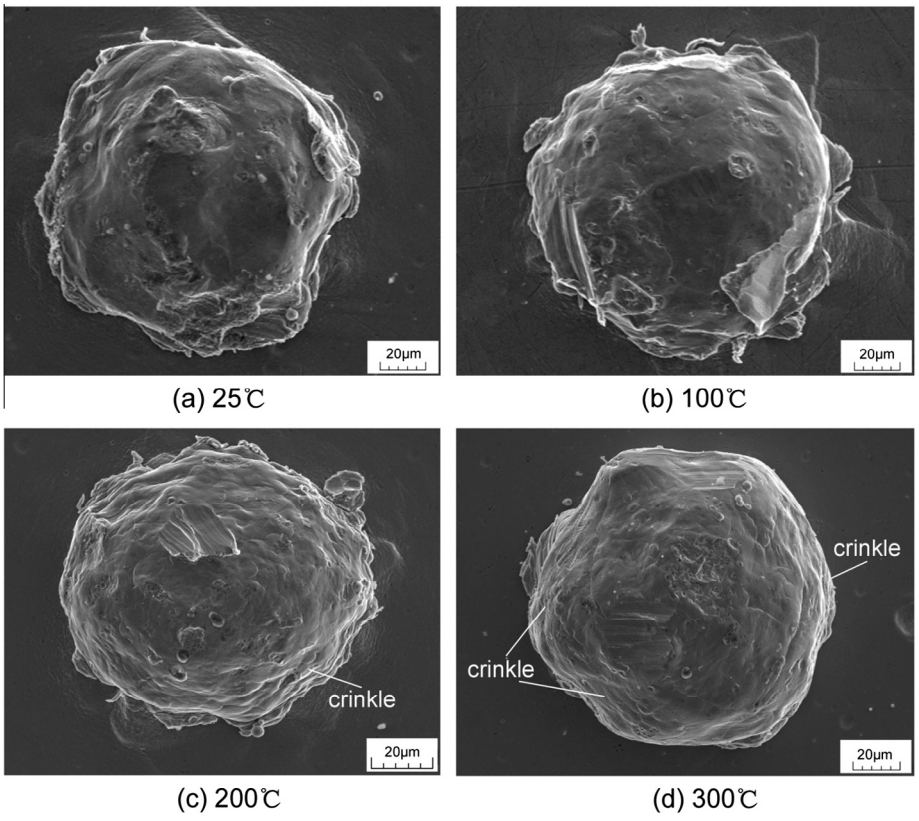

Fig. 13. Surface morphologies of a single splat observed by SEM as a function of the particle preheating temperature: (a) 25 °C, (b) 100 °C, (c) 200 °C and (d) 300 °C.

Moreover, Fig. 11 can also be used to explain why the adiabatic temperature rise decreases as the initial particle temperature increases. As already discussed in Section 3.2, the temperature rise is a consequence of plastic dissipation-induced adiabatic heating. Clearly, smaller plastic dissipation energy results in a lower adiabatic temperature rise. Therefore, the maximum temperature rise can decrease as the initial particle temperature increases as shown in Fig. 10.

Additionally, as shown in Fig. 11, it is interesting to find that the substrate plastic dissipation energy decreases gradually with increasing particle temperature. This is because the total plastic dissipation energy accounts for the overwhelming share among the four energies and the other three energies can be neglected. In this case, the plastic dissipation energy for different cases can be considered to have the same value due to the same initial kinetic energy. Accordingly, if the energy dissipated by the particle decreases with the particle temperature, the remaining energy allocated to the substrate should certainly follow an increasing trend.

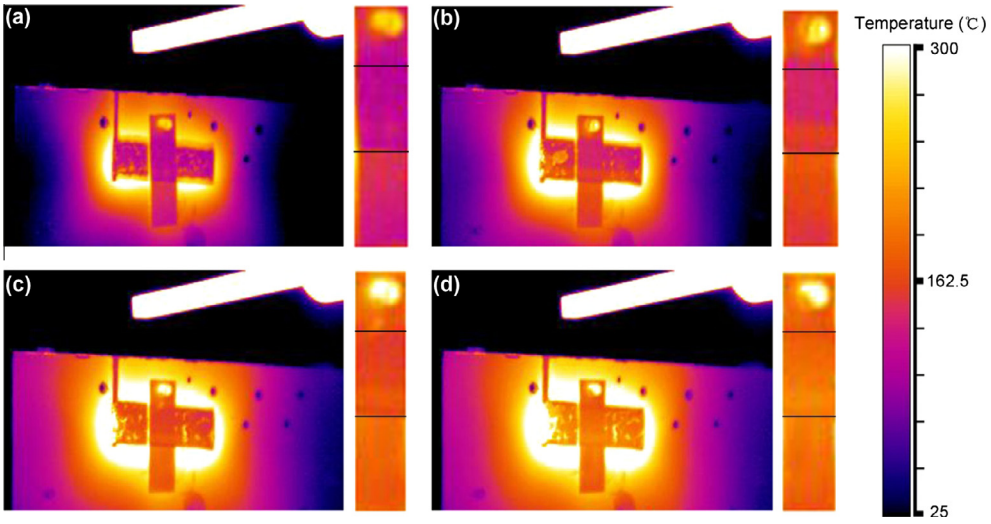

Fig. 14. Infrared images of the coating surface temperature after one-pass coating deposition as a function of the particle preheating temperature: (a) 25 °C, (b) 100 °C, (c) 200 °C and (d) 300 °C.

4.4. Splat observation

Fig. 12 displays the surface morphologies of the substrate following impact by several individual Cu particles with and without preheating treatment. It is clear that most of the particles can attach to the substrate surface after the high-velocity impact and all the successfully deposited particles exhibit a hemispheric outline. In addition, some craters can be clearly recognized on the substrate surface for non-preheating case as shown in Fig. 12a, while such craters are absent in the preheating case as indicated in Fig. 12b. Fig. 13 shows the surface morphologies of a single splat observed by SEM as a function of particle preheating temperature. As can be seen, for all cases, the Cu particle deforms hugely and flattens following deposition on the Cu substrate. For the non-preheating particle and preheating particle with relatively low temperatures of 100 and 200 °C, the metal jet from the substrate side can be clearly seen at the rim of the contact interface. However, for the particle with the preheating temperature of 300 °C, the substrate metal jet is hardly observed with only a small fraction exposed at the left side of the splat. This is because the thermal softening effect for the particle with the preheating temperature of 300 °C is very intense, enabling the particle to deform more easily and intensively. The metal jet, therefore, extends more remarkably and hides the substrate metal jet below the flattened splat. Furthermore, it can also be seen from Fig. 13 that some crinkle-like regions can be observed at the peripheral region of the splat surface as marked by the white lines. These crinkles result from the sudden solidification of the particle material which experiences plastic flow during the deposition process as a result of the dominant thermal softening effect over a fraction of the particle. These facts further confirm that particle preheating can enhance the thermal softening effect. If the preheating temperature is sufficiently high, plastic flow induced by the dominant thermal softening effect can occur over an even larger region, and not only at the interfacial region.

4.5. Coating performance

In the CS process, the final coating consists of several deposited layers. Every single layer is formed by the spray gun traveling only one pass through the sprayed target. Among these layers, except the first layer coating which deposits on the substrate surface, all of the following layers deposit directly on the previous formed coating. In this case, the already formed coating surface can be treated as the new sprayed target. In some studies, it is reported that increasing the substrate surface temperature can lead to higher deposition efficiency [38]. Therefore, it can be considered that the temperature of the already deposited coating may have some effects on the subsequent depositions. Fig. 14 shows infrared images of the coating surface temperature after one-pass coating deposition as a function of particle preheating temperature. It is clear that the coating surface temperature shows a roughly upward trend with increasing particle preheating temperature because the preheated particles can retain a relatively high temperature after deposition. More clearly, the average coating surface temperature of the corresponding samples is illustrated in Fig. 15. As can be seen, the average surface temperature of the coating formed by the non-preheated particles is about 116 °C, and with increasing the particle preheating temperature to 300 °C, the coating surface temperature can reach ~190 °C. This fact implies that particle preheating can lead to an increase in the coating surface temperature and enable the subsequently incident particles to deposit on an already heated surface. The result of this process is quite similar to the substrate preheating process in which the bonding strength and deposition efficiency

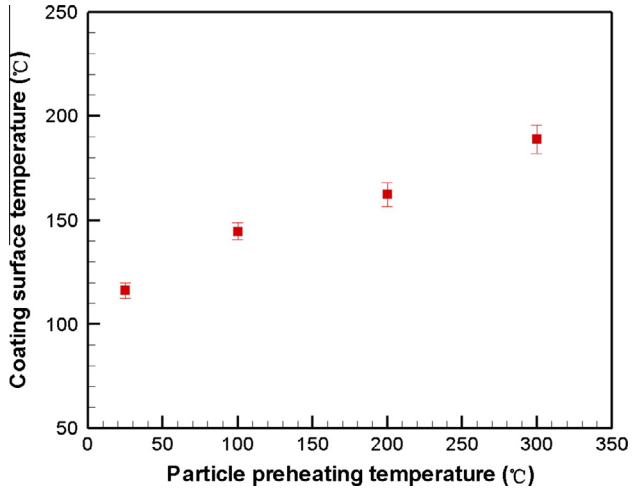

Fig. 15. Average coating surface temperature vs. the particle preheating temperature.

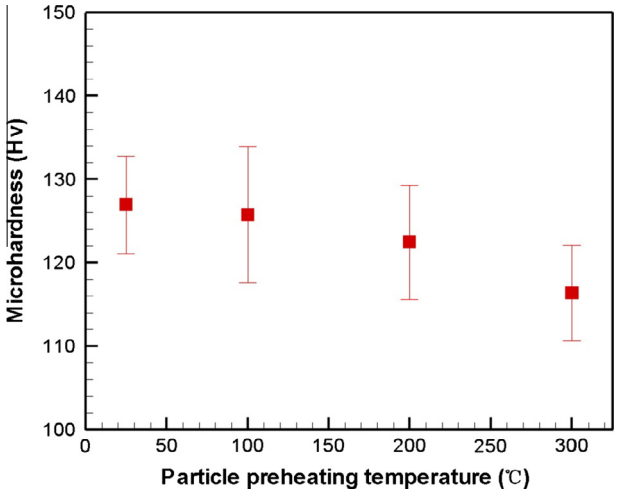

Fig. 17. Coating microhardness vs. particle preheating temperature.

increase with the substrate preheating temperature. Therefore, it is not difficult to conclude that particle preheating promotes coating quality due not only to the enhanced thermally softening effect of the particles but also to the high temperature of the coating surface. As the particle preheating temperature increases, the coating quality will become finer.

Fig. 16 shows cross-sectional OM micrographs of the cold-sprayed Cu coatings on Cu substrate with different particle preheating temperatures. Clearly, for each case, a relatively thick Cu coating can be formed on the Cu substrate without obvious porosity. However, with increasing the particle preheating temperature, the coating thickness shows an obvious upward trend, which further suggests that particle preheating does indeed promote the formation of a thick coating. Fig. 17 illustrates the effect of particle preheating temperature on the coating microhardness. As can be seen, with increasing the particle preheating temperature, the coating microhardness decreases gradually. This is because the thermal softening is enhanced with increasing preheating temperature. The enhanced thermal softening effect can eliminate any further work hardening effect, which partly contributes to the final coating hardness. Therefore, the coating microhardness exhibits a downward trend with increasing particle preheating temperature.

Fig. 18 shows cross-sectional OM micrographs of a single top-layer Cu particle as a function of the particle preheating temperature. Obviously, there exist some significant differences between different cases. For the non-preheating case as shown in Fig. 18a, the particle deforms to a limited extent and metal jet at the rim of

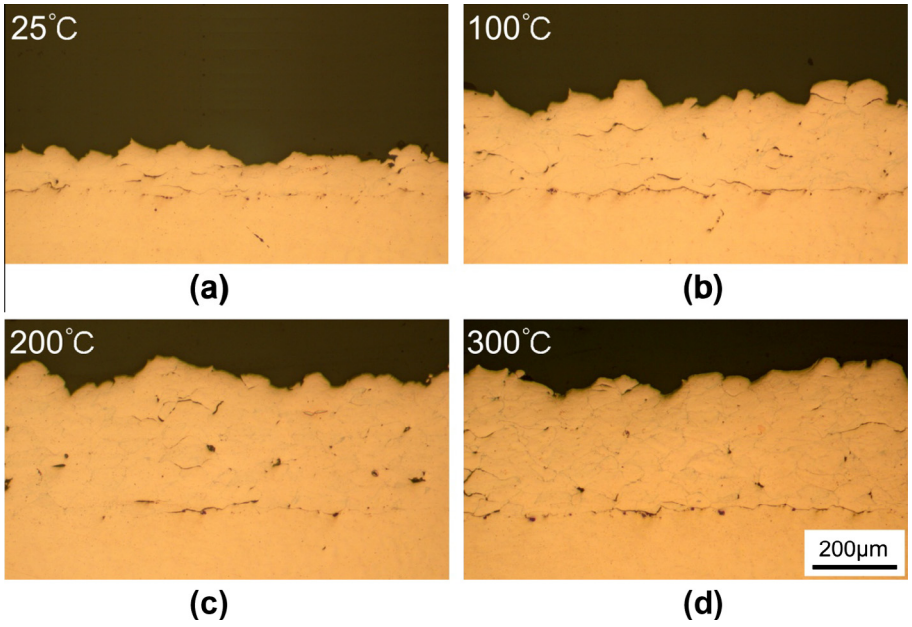

Fig. 16. Cross-sectional OM micrographs of the cold-sprayed Cu coatings on Cu substrate as a function of the particle preheating temperature: (a) 25 °C, (b) 100 °C, (c) 200 °C and (d) 300 °C.

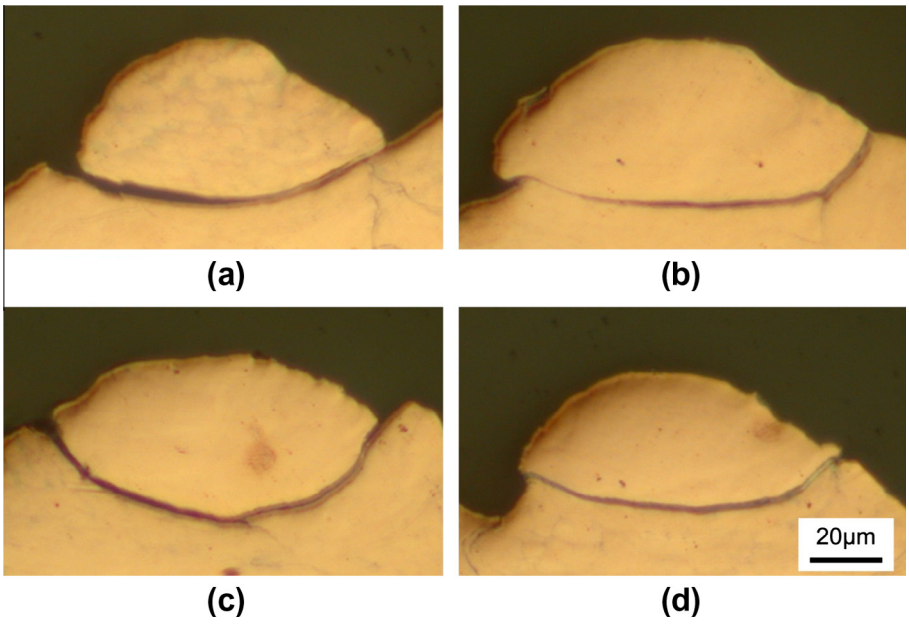

Fig. 18. Cross-sectional OM micrographs of a single top-layer Cu particle as a function of the particle preheating temperature: (a) 25 °C, (b) 100 °C, (c) 200 °C and (d) 300 °C.

the particle is difficult to observe. With increasing the particle preheating temperature to 100 °C, particle becomes more flattened but the outwards jet is still not prominent. Interestingly, it can be noticed that further increasing the particle preheating temperature to 200 °C results in the formation of the metal jet at the particle rim. Finally, when the preheating temperature reaches 300 °C, the metal jet becomes more intensive. The variation of particle deformation features with preheating temperature further implies that particle preheating can stimulate the formation of the viscous-like metal jet and confirms the FEA results in this study.

5. Conclusions

In the present investigation, the deposition behavior of thermally softened cold-sprayed particles was explored by the aid of a well-designed finite-element model in conjunction with experimental observation. For achieve the objective, relatively large Cu particles with different preheating temperatures were deposited on the Cu substrate, and both individual particle splats and full coating were obtained. Based on the predicted numerical results, a new concept, the TSZ, is proposed, which is defined as the local zone where the temperature is greater than $0.5T_m$, where thermal softening can occur. It is found that for non-preheating or low-temperature preheating particles, the TSZ is mainly localized at the narrow interfacial region, which means the thermal softening mainly occurs near the contact region. If the preheating temperature is sufficiently high, the TSZ can spread to the whole deformed particle, which indicates the whole particle can experience thermal softening. In addition, the simulation results also indicate that with increasing the particle initial temperature, particle will deform more and more intensively and the local maximum temperature increases gradually, due to the enhanced thermal softening effect. For high-temperature particles, a more prominent metal jet forms at the rim of the interface and the experimental observation on the individual particle splat confirms this finding. In addition, the experimental results also suggests that preheated particles are more likely to deposit on the substrate surface, while some craters are formed on the substrate surface when using non-preheated particles. As for the full coating formation process, the surface temperature of each layer coating increases gradually with particle preheating temperature. The increased coating surface temperature combined with the increased particle temperature can promote the formation of the cold-sprayed coatings and enable the formed coating to be rather thick. Moreover, due to the elimination of the work hardening by the thermal softening, the coating microhardness shows a decreasing trend with increasing particle preheating temperature.

Acknowledgment

The authors would like to acknowledge the support by Marie Curie FP7-IPACT-268696 (EU).

References

[1] Alkhimov AP, Kosareve VF, Papyrin AN. Doklady Akademii Nauk SSSR 1990;315:1062.
[2] Papyrin A. Adv Mater Process 2001;159:49.
[3] Assadi H. Acta Mater 2003;51:4379.
[4] Grujicic M, Zhao CL, DeRosset WS, Helfritch D. Mater Des 2004;25:681.

[5] Schmidt T, Gärtner F, Assadi H, Kreye H. Acta Mater 2006;54:729.
[6] Dykhuizen RC, Smith MF, Gilmore DL, Neiser RA, Jiang X, Sampath S. J Therm Spray Technol 1999;8:599.
[7] Grujicic M, Saylor JR, Beasley DE, DeRosset WS, Helfritch D. Appl Surf Sci 2003;219:211.
[8] Barradas S, Molins R, Jeandin M, Arrigoni M, Boustie M, Bolis C, et al. Surf Coat Technol 2005;197:18.
[9] Klinkov SV, Kosarev VF, Rein M. Aerosp Sci Technol 2005;9:582.
[10] Price TS, Shipway PH, McCartney DG, Calla E, Zhang D. J Therm Spray Technol 2007;16:566.
[11] Bae G, Xiong Y, Kumar S, Kang K, Lee C. Acta Mater 2008;56:4858.
[12] Bae G, Kumar S, Yoon S, Kang K, Na H, Kim H-J, et al. Acta Mater 2009;57:5654.
[13] Hussain T, McCartney DG, Shipway PH, Zhang D. J Therm Spray Technol 2009;18:364.
[14] Guetta S, Berger MH, Borit F, Guipont V, Jeandin M, Boustie M, et al. J Therm Spray Technol 2009;18:331.
[15] Yin S, Wang X-f, Li W-y, Xu B-p. J Therm Spray Technol 2009;18:686.
[16] Champagne VK, Helfritch D, Leyman P, Grendahl S, Klotz B. J Therm Spray Technol 2005;14:330.
[17] Wank A, Wielage B, Podlesak H, Grund T. J Therm Spray Technol 2006;15:280.
[18] Calvo FA, Urena A, Desalazar JMG, Molleda F. J Mater Sci 1988;23:2273.
[19] Manna I, Majumdar JD. J Mater Sci Lett 1993;12:920.
[20] Funamizu Y, Watanabe K. Trans Jpn Inst Met 1977;12:147.
[21] Lee H, Shin H, Ko K. J Therm Spray Technol 2009;19:102.
[22] Bolesta AV, Fomin VM, Sharafutdinov MR, Tolochko BP. Nucl Instrum Methods Phys Res, Sect A 2001;470:249.
[23] Barradas S, Guipont V, Molins R, Jeandin M, Arrigoni M, Boustie M, et al. J Therm Spray Technol 2007;16:548.
[24] King PC, Bae G, Zahiri SH, Jahedi M, Lee C. J Therm Spray Technol 2009;19:620.
[25] Wang H-T, Li C-J, Yang G-J, Li C-X. Appl Surf Sci 2008;255:2538.
[26] Wang H-T, Li C-J, Ji G-C, Yang G-J. J Therm Spray Technol 2012.
[27] Ning X-J, Jang J-H, Kim H-J. Appl Surf Sci 2007;253:7449.
[28] Shin S, Yoon S, Kim Y, Lee C. Surf Coat Technol 2006;201:3457.
[29] Kim K, Watanabe M, Kawakita J, Kuroda S. Scr Mater 2008;59:768.
[30] Kim K, Watanabe M, Kuroda S. Scr Mater 2009;60:710.
[31] Kim K, Watanabe M, Kuroda S. Surf Coat Technol 2010;204:2175.
[32] Li W-Y, Li C-J, Liao H. Appl Surf Sci 2010;256:4953.
[33] ABAQUS 6.11-2 user manual. Pawtucket: Hibbitt, Karlsson and Soerensen; 2011.
[34] Yin S, Wang X-F, Li W-Y, Xu B-P. J Therm Spray Technol 2010;19:1155.
[35] Johnson GR, Cook WH. A constitutive model and data for metals subjected to large strains, high strain rates and high temperatures. In: 7th Int symp on ballistics, The Netherlands; 1983. p. 541.
[36] Xu Y, Zhang J, Bai Y, Meyers MA. Metall Mater Trans A 2008;39:811.
[37] William FS, editor. Foundations of materials science and engineering. New York: McGraw-Hill; 1993.
[38] Fukumoto M, Wada H, Tanabe K, Yamada M, Yamaguchi E, Niwa A, et al. J Therm Spray Technol 2007;16:643.